PROCEEDINGS OF SPIE

SPIEDigitalLibrary.org/conference-proceedings-of-spie

Theoretical basis and experimental validation of harmonic coherence-based ultrasound imaging for breast mass diagnosis

Khadijat Kokumo, Arunima Sharma, Kelly Myers, Emily Ambinder, Eniola Oluyemi, et al.

Khadijat Kokumo, Arunima Sharma, Kelly Myers, Emily Ambinder, Eniola Oluyemi, Muyinatu A. Lediju Bell, "Theoretical basis and experimental validation of harmonic coherence-based ultrasound imaging for breast mass diagnosis," Proc. SPIE 12463, Medical Imaging 2023: Physics of Medical Imaging, 124630J (7 April 2023); doi: 10.1117/12.2655716

SPIE.

Event: SPIE Medical Imaging, 2023, San Diego, California, United States

Theoretical basis and experimental validation of harmonic coherence-based ultrasound imaging for breast mass diagnosis

Khadijat Kokumo[a], Arunima Sharma[b], Kelly Myers[c], Emily Ambinder[c], Eniola Oluyemi[c], and Muyinatu A. Lediju Bell[b,d,e]

[a]Department of Biomedical Engineering, Northwestern University, Evanston, IL
[b]Department of Electrical and Computer Engineering, Johns Hopkins University, Baltimore, MD
[c]Department of Radiology and Radiological Science, Johns Hopkins Medicine, Baltimore, MD
[d]Department of Computer Science, Johns Hopkins University, Baltimore, MD
[e]Department of Biomedical Engineering, Johns Hopkins University, Baltimore, MD

ABSTRACT

Coherence-based ultrasound imaging has demonstrated potential to improve breast mass diagnosis by distinguishing solid from fluid-filled masses. Harmonic imaging, which is known to reduce acoustic clutter, has the potential to offer additional improvements. However, the lack of a theoretical basis to describe these improvements precludes clinical recommendations based on physics and engineering principles. This work is the first to develop a theoretical model of coherence-based ultrasound imaging to describe both solid vs. fluid mass distinction and the effects of harmonic short-lag spatial coherence (SLSC) imaging. The scattering function and the transmit ultrasound beam of the van Cittert-Zernike theorem applied to ultrasound imaging were redefined to generate the theoretical model for solid vs. fluid mass distinction and for harmonic imaging, respectively. The derived theory was used to compare fundamental and harmonic SLSC images for hypoechoic solid, hypoechoic fluid, hyperechoic, and point targets. Theoretical simulations showed improved resolution, mitigated dark-region artifacts around hyperechoic targets, and increased spatial coherence of fluid masses in harmonic SLSC images when compared to fundamental SLSC images. Experimental data from tissue-mimicking phantoms and *in vivo* breast ultrasound images agreed with theoretical results. In particular, when compared to fundamental SLSC imaging, harmonic SLSC imaging improved resolution by 0.19 ± 0.25 mm, mitigated dark region artifacts by 0.55 ± 0.54 mm, and increased the spatial coherence of fluid-filled masses, resulting in a 6.50 ± 4.28 dB decrease in contrast. Results will enable future clinical recommendations supporting the use of fundamental or harmonic SLSC imaging for analyses of fluid or solid masses, respectively. These contributions establish a theoretical foundation to combine fundamental and harmonic coherence-based imaging with harmonic B-mode imaging to improve the accuracy of breast mass diagnoses.

Keywords: Breast ultrasound, ultrasonic imaging, harmonic imaging, coherence-based imaging

1. INTRODUCTION

Ultrasound imaging plays an important role in the detection of breast cancer, due to its portability, cost-effectiveness, and absence of ionizing radiation.[1] However, ultrasound is limited by its high false positive rates when discriminating benign from malignant masses and by the presence of acoustic clutter.[2,3] These challenges can cause important diagnostic features to be missed[2] and can also cause an overlap in the appearance of benign and malignant breast lesions, resulting in unnecessary follow-up exams and procedures.

Advances to improve existing limitations include harmonic imaging[4] and short-lag spatial coherence (SLSC) beamforming.[5] In harmonic imaging, pulses are transmitted at a fundamental frequency, and the higher harmonics of the received pulses are employed to create images. Harmonic ultrasound B-mode imaging is known to reduce clutter and improve lateral resolution, which improves diagnostic confidence.[6,7] SLSC beamforming is a

Address all correspondence to:
Muyinatu A. Lediju Bell, mledijubell@jhu.edu

Medical Imaging 2023: Physics of Medical Imaging, edited by Lifeng Yu, Rebecca Fahrig, John M. Sabol, Proc. of SPIE Vol. 12463, 124630J
 · 1605-7422 · doi: 10.1117/12.2655716

coherence-based imaging technique that measures and displays the similarity of closely separated backscattered ultrasound signals. SLSC imaging has been shown to reduce clutter and improve target boundary visibility when compared to traditional B-mode imaging.[8–10] In addition, SLSC imaging has been combined with harmonic imaging to offer additional improvements. For example, harmonic SLSC imaging of *in vivo* human liver[11,12] and cardiac[12,13] tissue suppresses acoustic noise, improves target detection, smooths tissue texture, and improves endocardial border visualization. Harmonic SLSC imaging has also improved target conspicuity[14] and border delineation within fetal ultrasound images.[9]

SLSC imaging and multiple SLSC-based imaging derivatives were recently employed to distinguish solid from fluid masses, demonstrating additional newfound potential to improve diagnostic accuracy when determining breast mass contents.[15–19] For example, Wiacek *et al.*[17] conducted a reader study with five board-certified breast radiologists, concluding that the incorporation of information from robust SLSC (R-SLSC) imaging reduced uncertainty in the diagnosis of fluid-filled masses from 47.5% to 15.8%, leading to a reduction of otherwise unnecessary biopsies from 33.3% to 13.3%. In addition, objective coherence-based metrics have been proposed to determine mass content without requiring reader input.[19,20]

While SLSC and harmonic imaging have independently been demonstrated to improve image quality and diagnostic capability, the integration of SLSC imaging with harmonic imaging was not previously combined to create breast images. Sharma *et al.*[19] produced related work combining R-SLSC and harmonic imaging, demonstrating that fundamental R-SLSC imaging is preferred over the newly investigated harmonic R-SLSC imaging to differentiate fluid-filled from solid masses due to the generally worse contrast of harmonic R-SLSC images when compared to fundamental R-SLSC images. However, the translatability of these findings to the more basic SLSC beamformer remains unclear. In addition, a theoretical basis is necessary to support this and related observations surrounding fundamental and harmonic SLSC imaging of solid and fluid-filled breast masses.

This paper introduces a theoretical model to describe and compare fundamental and harmonic SLSC imaging of different types of masses and other common imaging targets. We then compare theoretical observations to experimental data to validate our findings. With this development and validation, we discuss possible clinical implications of our results.

2. METHODS

2.1 Theoretical Simulations

SLSC imaging is based on the van Cittert-Zernike (VCZ) theorem applied to ultrasound imaging, which is described as follows at the ultrasound transmit focus:[5,21]

$$C = \left|\mathcal{F}\{{H_{tx}}^2 \cdot \chi^2\}\right|, \tag{1}$$

where C is spatial coherence as a function of spatial frequency, $\mathcal{F}$ denotes the Fourier transform, H_{tx} is the transmit ultrasound beam, modeled as a sinc function, and χ is the scattering function. Theoretical spatial coherence functions of fundamental data were obtained by evaluating Eq. (1) at spatial frequencies that coincide with the center transmit frequency of a simulated ultrasound transducer, using the same approach described in previous work.[5,21]

To develop a model for harmonic SLSC imaging, the H_{tx} term in Eq. (1) was redefined using the principle of acoustic reciprocity,[22] which dictates that the transmit beam profile is the same as the receive beam profile if the transmitter and receiver are interchanged and the surrounding acoustic environment otherwise remains the same. Using this principle, H_{tx} in Eq. (1) was redefined as the receive ultrasound beam, H_{rx}, resulting in the expression:

$$C = \left|\mathcal{F}\{{H_{rx}}^2 \cdot \chi^2\}\right|, \tag{2}$$

To develop a model for solid vs. fluid mass distinction, the χ term in Eqs. (1) and (2) was modified. Previous reports define χ as the source scattering function,[5,23] lateral backscatter profile,[5] or amplitude profile[21]. These definitions require careful reconsideration when masses have similar amplitude profiles and different coherence profiles (e.g., hypoechoic solid and hypoechoic fluid masses). In particular, scattering for a hypoechoic fluid mass is non-existent while scattering for the solid mass appears similar to tissue. Therefore, the scattering profile,

Table 1: Parameters for theoretical simulations

	Fundamental	Harmonic
Transmit frequency	6 MHz	-
Receive frequency	-	12 MHz
Transmit elements	94	-
Receive elements	-	94
Desired pitch	0.3 mm	0.3 mm
Image width	80 mm	80 mm
Imaging depth	38 mm	38 mm
M	10	10

χ, of a hypoechoic fluid mass was modeled as a constant with a lower coherence throughout the mass, when compared to the surrounding tissue, which is similar to previous theoretical models of hypoechoic masses.[5,24] Conversely, the scattering profile, χ, of a hypoechoic solid mass was modeled to be the same as previous models for diffuse scatterers (i.e., tissue),[5] with the addition of discontinuities at the lateral borders of the mass.

Eqs. (1) and (2) were also implemented to model a hyperechoic target and a point target. To create the hyperechoic target, the scattering profile was modelled as constant plus a rectangular pulse where the ratio of the pulse amplitude to the constant was equal to the contrast of the lesion and the width of the pulse was equal to the diameter of the lesion. To create the point target, the scattering function was modelled as constant plus a delta function (i.e., a constant with a single pixel having higher amplitude when compared to the constant).

For each of the four targets described above (i.e., hypoechoic solid, hypoechoic fluid, hyperechoic, and point targets), the normalized spatial coherence function, C, was integrated from lag value $m = 1$ to $m = M$:

$$R_{sl} = \int_{m=1}^{M} C(m)\, dm \;\approx \sum_{m=1}^{M} C(m)\,, \tag{3}$$

where the spatial lag, m, is proportional to the spatial frequency, u, through the wavelength associated with the transducer center frequency (i.e., λ), the imaging depth (i.e., z), and the transducer pitch. In particular,[21]

$$m = u\frac{\lambda z}{\text{pitch}}. \tag{4}$$

Based on this relationship, C in Eqs. (1) and (2) was numerically evaluated using the fast Fourier transform, then resampled based on the desired transducer pitch (i.e., the same approach described in previous work[5,21]). The fundamental or harmonic SLSC lateral line profile was then created by repeating this coherence function creation and integration process for multiple lateral positions, then each line profile was divided by M to normalize the final results. These theory-based simulations were implemented using MATLAB R2022a software with the specific parameters reported in Table 1.

2.2 Experimental Validation

Theoretical spatial coherence results were compared with results obtained from tissue-mimicking phantoms and *in vivo* breast imaging data acquisitions. Nine phantom images were acquired from the CIRS General Purpose Phantom Model 054GS (Norfolk, VA, USA). Of these nine images, two images consisted of a 12 dB hyperechoic target and the neighboring point targets, one image consisted of a 12 dB and a 6 dB hyperechoic target, one image consisted of three hyperechoic targets with contrast values of 12, 6, and 3 dB, two images consisted of point targets, and three images consisted of aneochoic targets. Five phantom images were acquired

Table 2: Parameters for experimental phantom and *in vivo* images.

	Phantom	*In vivo*
Transducer -6dB bandwidth	3-8 MHz	8-17 MHz
Transmit center frequency	3.5 MHz	6 MHz
Transmit elements	128	128
Receive elements	64	64
Pitch	0.3 mm	0.2 mm
Image width	38.2 mm	25.5 mm

from the CIRS Small Parts Ultrasound Phantom Model 050 (Norfolk, VA, USA). Of these five images, one image consisted of a 9 dB hyperechoic target, and four images consisted of point targets.

The *in vivo* breast data were acquired after receiving informed consent from six patients enrolled in an ongoing study approved by the Johns Hopkins Medicine Institutional Review Board (Protocol No. IRB00127110). The breast data consisted of four solid masses and two fluid-filled masses. The mass contents were verified post-image acquisition with aspiration and/or biopsy.

These data were acquired using an Alpinion ECUBE 12R (Alpinion, Seoul, Korea) ultrasound scanner, with the Alpinion L3-8 transducer used to acquire phantom data and the Alpinion L8-17 transducer used to acquire *in vivo* breast data. Transducer parameters associated with experimental data acquisitions are reported in Table 2. For each acquisition, the ultrasound transmit beam focus was varied to coincide with the target location.

A pulse-inversion sequence was transmitted to form matched fundamental and harmonic images. Echoes received from the normal pulses formed the fundamental channel data, while summed echoes received from normal and inverted pulses formed the harmonic channel data. These fundamental and harmonic channel data were delayed, then cross-correlated offline to create experimental spatial coherence functions using the equation:

$$C(m) = \frac{1}{N-m} \sum_{i=1}^{N-m} \frac{\sum_{n=n_1}^{n_2} s_i(n) s_{i+m}(n)}{\sqrt{\sum_{n=n_1}^{n_2} s_i^2(n) \sum_{n=n_1}^{n_2} s_{i+m}^2(n)}}, \tag{5}$$

where N is the number of elements in the transducer and $s_i(n)$ and $s_{i+m}(n)$ are the time-delayed signals at depth n. To form matched fundamental and harmonic SLSC images, Eq. (3) was applied to each experimental coherence function ($M = 10$), followed by normalization to the brightest pixel. Fundamental and harmonic SLSC images of the phantom data were displayed on a linear scale and *in vivo* data were displayed on a log scale after log compression. Corresponding fundamental and harmonic B-mode images were obtained by applying delay-and-sum beamforming to the fundamental and harmonic channel data, followed by envelope detection, normalization to the brightest pixel, and log compression.

Three metrics were computed and compared across matched fundamental and harmonic SLSC images to quantify image quality. First, the lateral full-width-at-half-maximum (FWHM) of point targets was measured to quantify lateral resolution. Second, we created a new metric called the full-width-at-half-minimum (FWHM-Min) to characterize and compare the size of dark regions surrounding hyperechoic targets, point targets, and solid *in vivo* masses. FWHM-Min is equal to width of a dark region at half of its minimum value. Third, the contrast of three images of the same anechoic cyst in the CIRS General Purpose Ultrasound Phantom and two fluid-filled *in vivo* masses was measured to characterize and compare the spatial coherence of hypoechoic masses in fundamental and harmonic SLSC images using the equation:

$$\text{Contrast} = 20 \log_{10} \left(\frac{S_i}{S_o} \right), \tag{6}$$

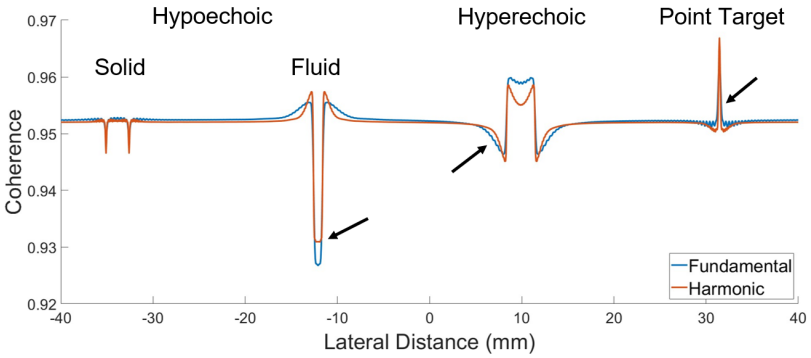

Figure 1: Line plots of hypoechoic solid, hypoechoic fluid, hyperechoic, and point targets created with theory-based fundamental and harmonic SLSC simulations.

where S_i is the mean amplitude of signals within the fluid region of interest (ROI) and S_o is the mean amplitude of signals within an ROI encompassing a background region located at the same depth as the target. These two circular ROIs were placed in the same location in matched fundamental and harmonic SLSC images. The diameters of the ROIs were 3 mm in the phantom images and either 2.6 mm or 2 mm in the *in vivo* fluid masses.

3. RESULTS

3.1 Qualitative Observations from Theoretical Simulations

Fig. 1 shows theoretical fundamental and harmonic SLSC lateral profiles for a solid hypoechoic mass, a fluid hypoechoic mass, a hyperechoic mass, and a point target, from left to right, respectively. Three qualitative observations based on the locations of the three arrows in Fig. 1 were derived from this plot. First, starting with the point target, a narrower point target width was achieved with harmonic SLSC imaging when compared to fundamental SLSC imaging. This observation is expected to translate to an improved point target resolution with harmonic SLSC imaging compared to fundamental SLSC imaging. Second, moving to the hyperechoic target, note the lower spatial coherence surrounding this target relative to the baseline coherence values that exist outside of this region. This region is expected to appear with the darkest pixel values in SLSC images, and they also have a wider profile with fundamental SLSC imaging compared to harmonic SLSC imaging. This observation is expected to translate to the reduced appearance of dark regions in harmonic SLSC images compared to fundamental SLSC images. Third, the hypoechoic fluid mass has greater spatial coherence with harmonic SLSC imaging when compared to fundamental SLSC imaging.

3.2 Resolution of Point Targets

Fig. 2 shows an example of matched fundamental (Fig. 2(a)) and harmonic (Fig. 2(b)) SLSC images of point targets acquired using the CIRS General Ultrasound Phantom. Eleven point targets in the focal zone of eight phantom images were utilized to compute FWHM, including the point target indicated by the arrows. A bar graph of the measured FWHM of the 11 point targets is displayed in Fig. 2(c). Harmonic SLSC imaging generally has a reduced FWHM when compared to fundamental SLSC imaging (mean $\pm$ one standard deviation reduction of 0.19 $\pm$ 0.25 mm), demonstrating that harmonic SLSC imaging generally improves resolution when compared to fundamental SLSC imaging. The improved resolution of harmonic SLSC imaging compared to fundamental SLSC imaging agrees with the first theoretical observation in Section 3.1.

3.3 Mitigation of Dark Regions Surrounding Hyperechoic Targets and Solid Masses

Fig. 3(a) shows an example of matched fundamental and harmonic B-mode and SLSC images of an *in vivo* solid mass. The arrows indicate dark regions at the boundaries of this solid mass. These dark regions were not present as a distinct feature in the corresponding B-mode images, thus they are considered artifacts of the nonlinear coherence imaging process. A total of 8 dark-region artifacts were identified in the SLSC images of

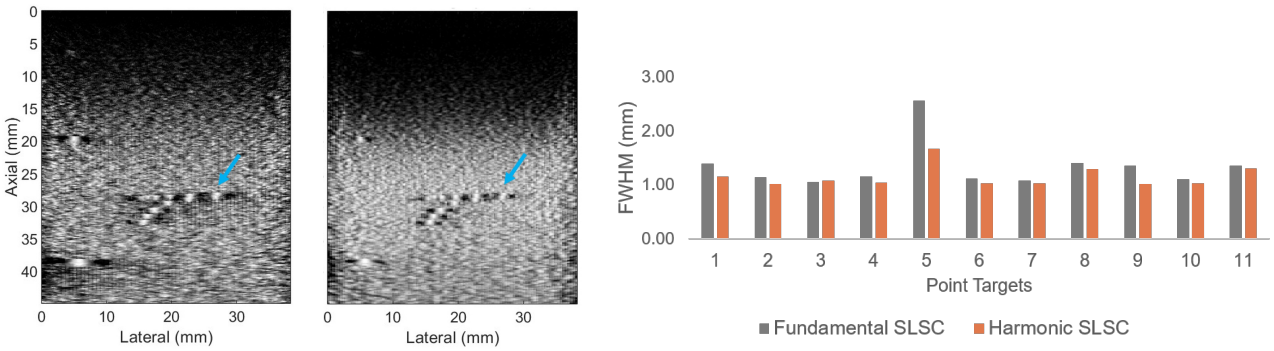

(a) (b) (c)

Figure 2: (a) Fundamental and (b) harmonic SLSC images (M = 10) of lateral point targets from phantom data, displayed on a linear scale ranging 0 to 1. The arrows denote one of the point targets utilized to compute FWHM. (c) Lateral FWHM of point targets identified in eight phantom images.

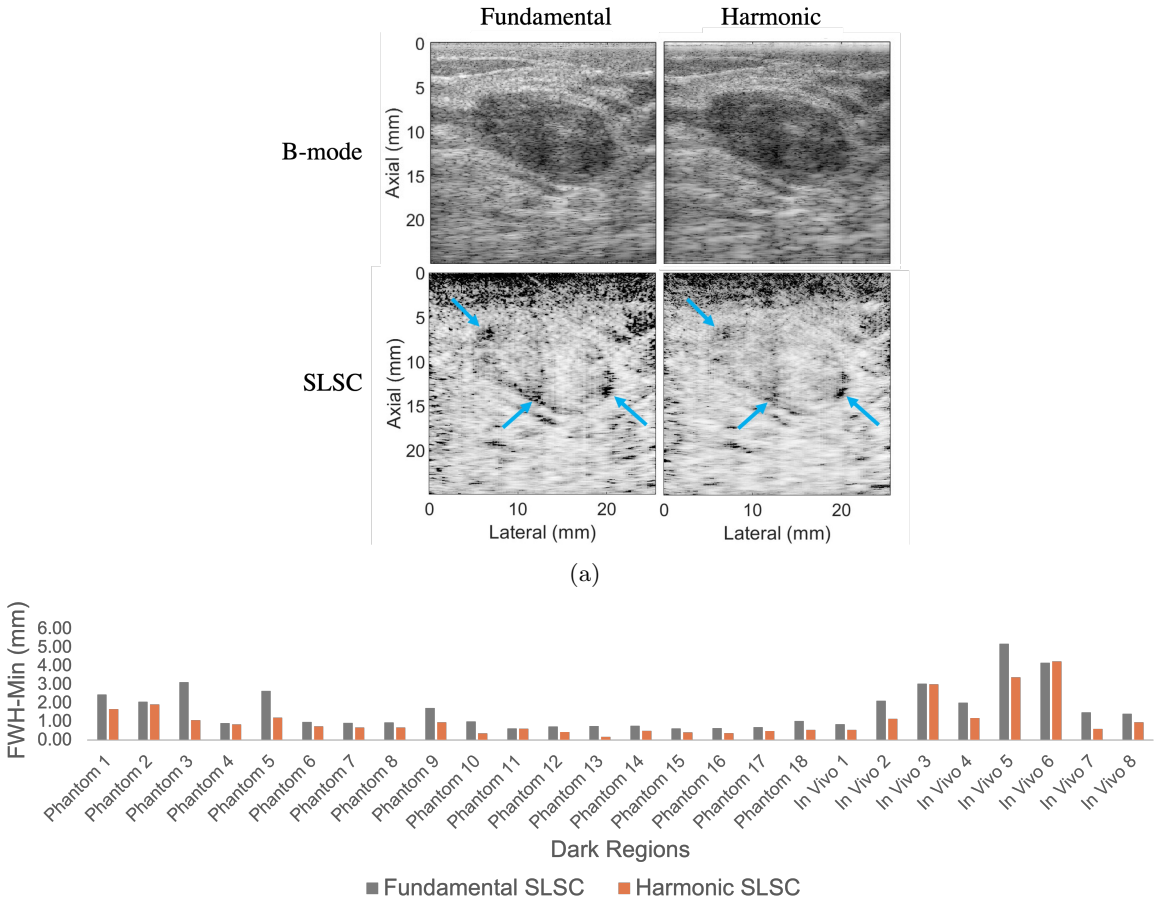

(a)

(b)

Figure 3: (a) Fundamental and harmonic delay-and-sum B-mode images with simultaneously acquired fundamental and harmonic SLSC images (M = 10) of an *in vivo* solid mass, each displayed with 60 dB dynamic range. Arrows denote identified dark region artifacts. (b) FWH-Min of 26 dark region artifacts identified in phantom and *in vivo* SLSC images.

the four acquired solid hypoechoic *in vivo* masses. In addition, 18 dark regions surrounding hyperechoic and point targets in the 11 acquired phantom images were also identified. A bar graph of the measured FWH-Min of these 26 dark region artifacts is displayed in Fig. 3(b). The FWH-Min generally decreased with harmonic SLSC imaging when compared to fundamental SLSC imaging by a mean ± one standard deviation of 0.55 ± 0.54 mm. Both qualitative observations and quantitative data presented in Fig. 3 agree with the second observation from the theoretical results presented in Section 3.1. In particular, harmonic SLSC imaging reduces the appearance of dark region artifacts present in fundamental SLSC images.

3.4 Spatial Coherence within Fluid Masses

Fig. 4 shows an example of matched fundamental and harmonic SLSC images of a fluid-filled *in vivo* mass. The spatial coherence within the fluid region appears to have increased in the harmonic SLSC image when compared to the corresponding fundamental SLSC image. As the spatial coherence of tissue is typically greater than that of a fluid-filled mass, an increase in spatial coherence is expected to be quantified with a reduced contrast. A bar graph of the measured contrast of three fluid-filled regions in phantom data and two fluid-filled regions within *in vivo* data is displayed in Fig. 4(c). The mean ± one standard deviation of differences in contrast between fundamental and harmonic SLSC images was 6.50 ± 4.28 dB. The decreased contrast with harmonic SLSC imaging corresponds to the increase in spatial coherence observed within fluid-filled hypoechoic regions in harmonic SLSC images, and the quantitative result supports the third observation reported in Section 3.1. In particular, harmonic SLSC imaging increases the spatial coherence within the fluid mass when compared to fundamental SLSC imaging.

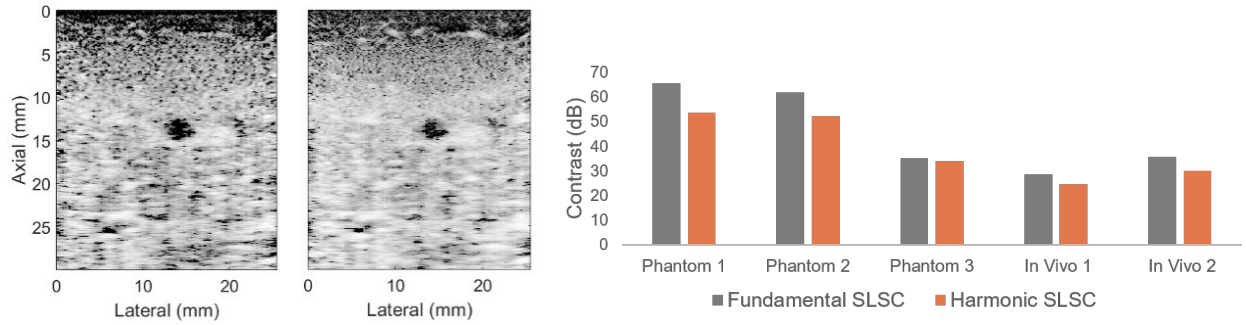

(a) (b) (c)

Figure 4: (a) Fundamental and (b) harmonic SLSC images (M = 10) of an *in vivo* fluid-filled mass, each displayed with 60 dB dynamic range. (c) Measured contrast of five fluid-filled regions in phantom and *in vivo* data.

4. DISCUSSION

This work is the first to develop a theoretical model of coherence-based ultrasound imaging to describe both solid vs. fluid-filled mass distinction and the effects of harmonic SLSC imaging. The combination of SLSC imaging and harmonic imaging to create breast images was also presented for the first time in this paper. Three observations from theoretical results were shown to generally agree with experimental observations. While harmonic imaging is generally thought to reduce clutter and is often considered as the preferred imaging approach with B-mode imaging, we provide the evidence and associated rationale to support that harmonic spatial coherence imaging is not always the preferred approach for the distinction of fluid-filled from solid masses, particularly due to the increased spatial coherence and poorer contrast observed in fluid-filled masses created with this approach.

Experimental validation of the three observations surrounding the resolution, dark-regions, and coherence of harmonic SLSC images serves as a foundation for future clinical recommendations. These results support the use of fundamental or harmonic coherence imaging alongside B-mode imaging for assessment of the fluid or solid content of breast masses (with possible extension to masses in other organs). In particular, a combination of harmonic B-mode and harmonic coherence imaging seems most likely to be useful when identifying the presence

of a solid mass. This combination would enhance mass visualization, while also ensuring solid content, based on the second observation that harmonic SLSC imaging mitigates the dark region artifacts surrounding solid masses when compared to fundamental SLSC imaging. However, for a fluid-filled mass, a combination of harmonic B-mode and fundamental SLSC imaging seems more likely to be useful, as harmonic imaging reduces acoustic clutter (compared to fundamental B-mode images), which is likely responsible for the increased spatial coherence within the harmonic SLSC images of fluid-filled masses (compared to fundamental SLSC images), resulting in the fluid content of these masses appearing less certain. This clinical observation is supported by contrast measurements in experimental data and by the third theoretical observation that harmonic coherence imaging increases the spatial coherence within fluid-filled masses.

The conclusions and clinical recommendations based on the contrast of fluid-filled regions in harmonic SLSC breast images may differ when compared to contrast measurements previously achieved in other organs. We offer the following two observations regarding these differences. First, contrast values highly depend on ROI selection. Previous work[9,11,12,25] appears to have selected ROIs in visually improved regions, and this selection aptly supports related conclusions that harmonic SLSC imaging improves contrast when compared to fundamental SLSC imaging. Second, harmonic imaging is known to improve visualization of deep structures, due to nonlinear propagation being underdeveloped in the near-field region of the ultrasound beam.[26] Because the distance between the transducer and a breast mass (e.g., 1-2 cm) is generally less than the distance to a fetus or the liver (e.g., 10-12 cm for fetal imaging), the positive effects of harmonic SLSC imaging compared to fundamental SLSC imaging seem to be more prominent in fetal[9,25] and liver[12] imaging than in breast imaging. However, there are also *in vivo* liver cases in which the contrast gains with harmonic SLSC imaging were marginal (i.e., 0.1 dB increase) or minimally worse (i.e., -2 dB decrease) when compared to matched fundamental SLSC images.[11]

5. CONCLUSION

We present a new theoretical basis to support clinical recommendations based on physics and engineering principles when visualizing fluid-filled and solid masses with harmonic coherence imaging. Our theory-based observations were supported by experimental data, which showed that harmonic imaging improved resolution by 0.19 $\pm$ 0.25 mm, mitigated dark region artifacts by 0.55 $\pm$ 0.54 mm, and reduced the certainty of fluid contents when compared to fundamental imaging, resulting from a 6.50 $\pm$ 4.28 dB decrease in contrast. These contributions establish a theoretical foundation to combine fundamental and harmonic coherence-based imaging with harmonic B-mode imaging to improve the accuracy of breast mass diagnosis.

ACKNOWLEDGMENTS

This work is supported by the National Institute of Biomedical Imaging and Bioengineering of the National Institutes of Health under Award Number R01EB032960. This work was also completed in partnership with the NSF Computational Sensing and Medical Robotics Research Experience for Undergraduates program (NSF Grant No. EEC-1852155). The authors thank Dr. Alycen Wiacek for acquiring phantom data, for assisting with patient data acquisition and consent, and for her involvement in initial discussions surrounding dark region artifacts.

REFERENCES

[1] Kaplan S. S, "Clinical utility of bilateral whole-breast US in the evaluation of women with dense breast tissue," *Radiology* **221**(3), 641–649 (2001).

[2] Lediju M. A, Pihl M. J, Dahl J. J, and Trahey G. E, "Quantitative assessment of the magnitude, impact and spatial extent of ultrasonic clutter," *Ultrasonic Imaging* **30**(3), 151–168 (2008).

[3] Entrekin R. R, Porter B. A, Sillesen H. H, Wong A. D, Cooperberg P. L, and Fix C. H, "Real-time spatial compound imaging: Application to breast, vascular, and musculoskeletal ultrasound," *Seminars in Ultrasound, CT and MRI* **22**(1), 50–64 (2001).

[4] Tranquart F, Grenier N, Eder V, and Pourcelot L, "Clinical use of ultrasound tissue harmonic imaging," *Ultrasound in Medicine & Biology* **25**(6), 889–894 (1999).

[5] Lediju M. A, Trahey G. E, Byram B. C, and Dahl J. J, "Short-lag spatial coherence of backscattered echoes: Imaging characteristics," *IEEE Transactions on Ultrasonics, Ferroelectrics, and Frequency Control* **58**(7), 1377–1388 (2011).

[6] Averkiou M, "Tissue harmonic imaging," in [*2000 IEEE Ultrasonics Symposium. Proceedings. An International Symposium (Cat. No.00CH37121)*], **2**, 1563–1572 (2000).

[7] Ward B, Baker A. C, and Humphrey V. F, "Nonlinear propagation applied to the improvement of resolution in diagnostic medical ultrasound," *The Journal of the Acoustical Society of America* **101**(1), 143–154 (1997).

[8] Lediju Bell M. A, Goswami R, J. A. Kisslo J. J. D, and Trahey G. E, "Short-lag spatial coherence imaging of cardiac ultrasound data: Initial clinical results," *Ultrasound in Medicine & Biology* **39**(10), 1861–1874 (2013).

[9] Kakkad V, Dahl J, Ellestad S, and Trahey G, "*In vivo* application of short-lag spatial coherence and harmonic spatial coherence imaging in fetal ultrasound," *Ultrasound in Medicine & Biology* **37**(2), 101–116 (2015).

[10] Jakovljevic M, Trahey G. E, Nelson R. C, and Dahl J. J, "Clinical utility of fetal short-lag spatial coherence imaging," *Ultrasound in Medicine & Biology* **44**(4), 794–806 (2018).

[11] Jakovljevic M, Trahey G. E, Nelson R. C, and Dahl J. J, "In vivo application of short-lag spatial coherence imaging in human liver," *Ultrasound in Medicine & Biology* **39**(3), 534–542 (2013).

[12] Dahl J. J, Jakovljevic M, Pinton G. F, and Trahey G. E, "Harmonic spatial coherence imaging: An ultrasonic imaging method based on backscatter coherence," *IEEE Transactions on Ultrasonics, Ferroelectrics, and Frequency Control* **59**(4), 648–659 (2012).

[13] Bell M. A. L, Goswami R, Dahl J. J, and Trahey G. E, "Improved visualization of endocardial borders with short-lag spatial coherence imaging of fundamental and harmonic ultrasound data," in [*2012 IEEE International Ultrasonics Symposium*], 2129–2132 (2012).

[14] Long W, Hyun D, Choudhury K. R, Bradway D, McNally P, Boyd B, Ellestad S, and Trahey G. E, "Clinical utility of fetal short-lag spatial coherence imaging," *Ultrasound in Medicine & Biology* **44**(4), 794–806 (2018).

[15] Wiacek A, Rindal O, Falomo E, Myers K, Fabrega-Foster K, Harvey S, and Bell M. A. L, "Robust short-lag spatial coherence imaging of breast ultrasound data: Initial clinical results," *IEEE Transactions on Ultrasonics, Ferroelectrics, and Frequency Control* **66**(3), 527–540 (2019).

[16] Wiacek A, Falomo E, Myers K, Hoel Rindal O. M, Fabrega-Foster K, Harvey S, and Bell M. A. L, "Clinical feasibility of coherence-based beamforming to distinguish solid from fluid hypoechoic breast masses," in [*2018 IEEE International Ultrasonics Symposium*], 1–4 (2018).

[17] Wiacek A, Oluyemi E, Myers K, Mullen L, and Bell M. A. L, "Coherence-based beamforming increases the diagnostic certainty of distinguishing fluid from solid masses in breast ultrasound exams," *Ultrasound in Medicine & Biology* **46**(6), 1380–1394 (2020).

[18] Wiacek A, Oluyemi E, Myers K, Mullen L, and Bell M. A. L, "Coherence-based beamforming improves the diagnostic certainty of breast ultrasound exams," in [*2020 IEEE International Ultrasonics Symposium*], 1–4 (2020).

[19] Sharma A, Wiacek A, Oluyemi E, Myers K, Ambinder E, and Bell M. A. L, "Distinguishing fluid and solid breast masses with fundamental and harmonic amplitude- and coherence-based ultrasound beamforming," in [*2022 IEEE International Ultrasonics Symposium*], (2022).

[20] Wiacek A, Oluyemi E, Myers K, Ambinder E, and Bell M. A. L, "Coherence metrics for reader-independent differentiation of cystic from solid breast masses in ultrasound images," *Ultrasound in Medicine & Biology* **49**(1), 256–268 (2023).

[21] Lediju Bell M. A, Dahl J. J, and Trahey G. E, "Resolution and brightness characteristics of short-lag spatial coherence (SLSC) images," *IEEE Transactions on Ultrasonics, Ferroelectrics, and Frequency Control* **62**(7), 1265–1276 (2015).

[22] Bottenus N and Üstüner K. F, "Acoustic reciprocity of spatial coherence in ultrasound imaging," *IEEE Transactions on Ultrasonics, Ferroelectrics, and Frequency Control* **62**(5), 852–861 (2015).

[23] Mallart R and Fink M, "The van Cittert–Zernike theorem in pulse echo measurements," *The Journal of the Acoustical Society of America* **90**, 2718–2727 (1991).

[24] Dahl J. J, Hyun D, Lediju M. A, and Trahey G. E, "Lesion detectability in diagnostic ultrasound with short-lag spatial coherence imaging," *Ultrasonic Imaging* **33**(2), 119–133 (2011).

[25] Kakkad V, Dahl J, Ellestad S, and Trahey G, "In vivo performance evaluation of short-lag spatial coherence and harmonic spatial coherence imaging in fetal ultrasound," in [*2013 IEEE International Ultrasonics Symposium*], 600–603 (2013).

[26] Muir T and Carstensen E, "Prediction of nonlinear acoustic effects at biomedical frequencies and intensities," *Ultrasound in Medicine & Biology* **6**(4), 345–357 (1980).